J. Condensed Matter Nucl. Sci. 20 (2016) 1–28

Research Article

Attempted Replication of Excess Heat in the Letts Dual-laser Experiment

Mason J. Guffey, Yang Tang and P.J. King*

ReResearch LLC, 3519 Jack Northrop Ave., Hawthorne, CA 90250, USA

Abstract

By attempting a nearly exact replication of prior published work, we test the claim that release of non-chemical excess heat from loaded palladium deuteride (PdD) can be triggered by the application of two laser beams with wavelengths selected at specific difference frequencies around 8, 15 and 20 THz. No significant excess heat events were observed in 231 laser triggered trials across 9 cathode runs. The average excess heat rate observed from all runs was 6.1 ± 21.6 mW with $\sim$10 W of input electrical power. We found no evidence of excess heat on the order of 100 mW reported by Letts. Calorimetry artifacts stemming from apparatus design issues often exceeded 100 mW and contributed to larger-than-desired uncertainties on individual excess heat measurements.
 ISSN 2227-3123

Keywords: Dual-laser experiment, Phonon, THz, Triggering

1. Introduction

The March 23, 1989 announcement by Martin Fleischmann and Stanley Pons of the possibility of nuclear fusion in an electrochemical system of heavy water (D_2O) and Pd generated worldwide interest [1–3]. Since then, small groups of researchers have been trying to replicate these claims without definitive success. Some experimental observations of anomalous heat effects (AHE) were made using calibrated calorimetry [4]. Others have claimed the correlated generation of He as a reaction byproduct [5], thus lending credence to the conjecture that a nuclear reaction may be taking place in the system.

Unfortunately, almost no published reports describe the specific steps necessary to independently reproduce claims of AHE reliably starting from commercially available materials and equipment. While preparation of the Pd cathode is proposed to be a crucial determinant of success [6], descriptions of specific cathode preparation procedures along with quantitative material properties are rare. Furthermore, there is no consensus within the research community about what kind of material preparation is required to observe the effect.

The dual-laser experiment (DLE) published by Dennis Letts [7,8] is a rare example of a report of AHE combined with sufficient documentation for a replication attempt. The reports of Letts et al. claim that a sufficiently prepared

*Corresponding author. E-mail: pjking@reresearch.net.

 ISSN 2227-3123

Pd cathode plated with Au will exhibit excess heat on the order of 100–300 mW in response to stimulation by two lasers having a frequency difference tuned to specific peaks in the THz range. These peaks coincide with phonon resonance frequencies of Pd, making the reports even more remarkable. Letts et al. [7,8] document the specific material preparation and measurement steps making a high fidelity replication attempt feasible. Letts claimed a 95% replication rate of AHE by following his protocol [8].

The DLE merits replication for another reason: the low energy nuclear reactions research community considers it an important result to build upon. For example, it provides experimental support for Peter Hagelstein's theoretical explanations of AHE, and it was referenced at least twice in oral presentations at the International Conference on Condensed Matter Nuclear Science (*ICCF-19*) in April 2015 [9,10].

This report describes our attempt to replicate the DLE, based on published reports and limited additional input from Letts. We did not observe the laser-triggered excess heat effects described by Letts et al. but we learned a lot about the experimental apparatus. We speculate on possible reasons for our different result, and suggest ways in which the DLE could be improved to make other replication attempts more straightforward.

2. Experiment

Letts concluded a 2015 publication [8] with the following:

"The dual-laser experiments seem to support these conclusions:

(1) Three specific beat frequencies will trigger excess power in a deuterated cathode.
(2) Cathode fabrication, loading and laser application protocols enable excess power.
(3) An external magnetic field is required and its affect (sic) is linear.
(4) Polarization of the laser beams affects excess power.
(5) Plating gold on the cathode surface after loading is required to produce excess power.
(6) Higher cell temperature produces larger excess power and is exponential in effect.
(7) The dual-laser effect is highly reproducible when protocols are followed."

Our experimental procedure was designed to closely replicate the protocol described in Letts JCMNS 2010, with additional input obtained via personal correspondence with Letts [11]

2.1. Materials preparation

Letts suggested that we use the 17-step procedure provided in his ASTI 2004 presentation [12] as our principal guide for cathode preparation. The 17 steps are summarized below:

Step 1 : The starting material was 0.5 mm thick palladium foil, *Alfa Aesar #11514* (99.9% purity metals basis). A piece of the material, $\sim$10 mm $\times$ 8 mm in size was cut from the foil with the use of a *Dremel rotary tool* with a *diamond wheel cutter* attachment.

Step 2 : This piece is polished using a polishing compound (*Custom Chemical Packaging Pol-Gel*, a rebranded version of the 10,000 grit Nicsand used in the original work) and the Dremel tool first with a metal and then with a fiber brush attachment. The polishing generally results in a mirror-like finish.

Step 3 : The resulting piece is rinsed in either tap or distilled water.

Step 4 : The piece is then annealed in a benchtop furnace (*Thermolyne type 1300*) to 750°C for 3 h, then allowed to cool in air overnight. This procedure and all subsequent annealing steps result in a blue-green surface sheen attributed to oxide.

Step 5 . Next the piece was etched in aqua regia (1:3 HNO_3:HCl) for 2–10 min. It was found that some degree of variability resulted from this procedure, in some instances completely removing the oxide layer and resulting in a speckled shiny surface, while in other instances the oxide coating was incompletely removed. In some instances the aqua regia was used after waiting a few hours as was the standard procedure known to the author, while in others it was used immediately after mixing on instructions from Letts [9].

Step 6 . After etching, the piece is washed in distilled water, then re-polished using the same procedure as above (Steps 2 and 3).

Step 7 : Repeat Step 6.

Step 8 . The piece is then cleaned in an ultrasonic bath with distilled water for 5 min, then. . .

Step 9 : . . . annealed at 850°C for 2.5 h and allowed to cool overnight.

Step 10 : Afterwards, the piece is re-polished (resulting in the removal of the oxide film) and . . .

Step 11 : . . . ultrasonically cleaned in either 1:1 H_2O:IPA or a ∼15% solution of *Cole-Parmer ultrasonic compound remover* . The decision to use the former was based on the procedure's description of "compound remover", the latter was used based on the specific suggestion of Letts [9].

Step 12 : Next the piece was cold-rolled with a *Woodward Fab slip roller* cleaned with acetone prior to each use. Several passes through the roller (∼5–10) were necessary to achieve the target thickness of 250 μm specified in the procedure, verified with a set of calipers. The piece was rotated 90° each pass through the roller.

Step 13 : Subsequent to the rolling, the piece is polished, . . .

Step 14 : . . . ultrasonically cleaned (Step 8), . . .

Step 15 : . . . annealed at 850°C (Step 9), and

Step 16 : . . . etched in aqua regia as described previously (Step 5).

Step 17 : The piece is then ready to be cut into 2–3 rectangular coupons 5 mm × 10 mm in size for use in the experiment.

The final wash applied to the sample varied between experiments, see Supplemental Information for details.

2.1.1. *Cathode material supplied by Letts*

For one experiment (DLER7), cathode material was supplied directly by Letts, from a batch that had successfully produced excess heat from the dual-laser effect in his May 2012 experiment. In two other runs (DLER10 and DLER11), the material was processed by us, except for the final etch (Step 16 above), which was performed by Letts. See Table 1 for experimental designations.

2.1.2. *Cathode material supplied by Coolescence LLC*

For experiment DLER17, the cathode material was supplied by Coolescence LLC. The foil sample was mechanically mounted in a PEEK (polyether ether ketone) assembly during measurement.

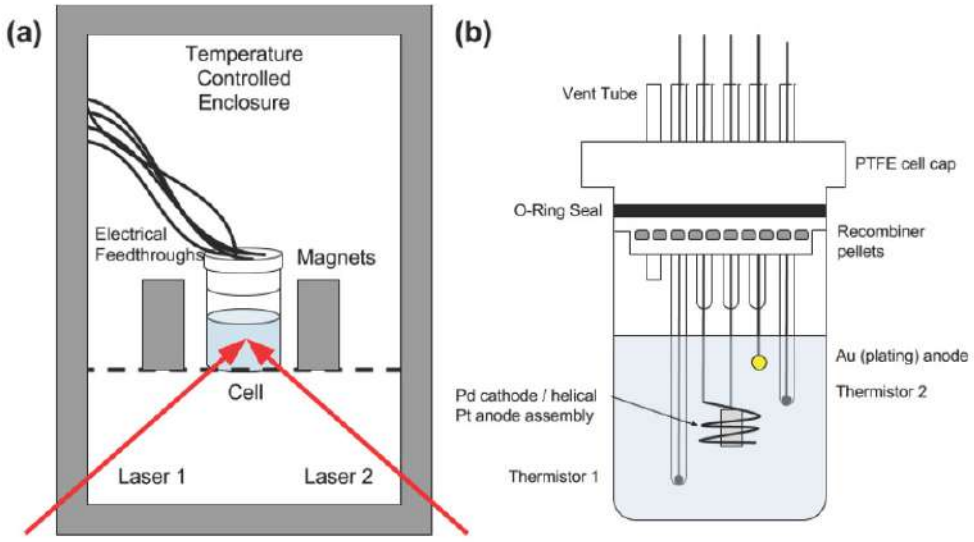

Figure 1. (a) A depiction of the entire apparatus. The cell and magnets rest on a wire frame grating of the temperature enclosure. See Supplementary Information for more details. (b) The measurement cell. For 4-wire resistance measurement, four additional wires were connected to cathode. These are omitted from the figure for clarity.

2.2. Setup description

Experiments were conducted in a custom-built, temperature controlled enclosure consisting of a modified commercial beverage cooler outfitted with a system of fans and baffles to circulate air, and a heating wire controlled with a Keysight E3632A power supply (see Supplemental Information). The enclosure temperature was determined from an average of either two or four thermistors located inside the enclosure, and a software-controlled PID loop controlled the heater wire voltage using this input.

The cell consisted of a 300 mL borosilicate lab beaker (Kimble KIMAX #14020) with a custom-built Teflon cell cap (see Fig 1 and Supplemental Information). Feedthroughs for temperature probes were constructed by taking 5 mm OD glass tubing (Ginsberg Scientific #5MMSLT-24) and sealing one end completely with a butane torch. Into these tubes were inserted *Measurement Specialties 44004RC* thermistors, and the back end of the tube was sealed with superglue. Feedthroughs for the three electrodes (the Pd cathode, and the Pt and Au anodes) were constructed as follows: First, a piece of 500 μm diameter Pt wire (Alfa Aesar #43288) was soldered onto Cu wire. Then one end of a piece of glass tubing was sealed around the Pt wire. Next, the wire was either laser-welded onto the Pd cathode, shaped into a coil for the Pt anode, or in the case of the Au anode a small bunch of Au wire (*Alfa Aesar #10968*) was melted onto the end of the Pt wire. A depiction of the entire apparatus (cell plus enclosure) is shown in Fig. 1.

Cell current was provided by a second Keysight E3632A power supply. The thermistors were measured with a digital multimeter/switch combination from National Instruments, models *PXI-4070* and *PXI-2503*. Temperature measurements were conducted using built-in LabVIEW routines for thermistor measurement at 10 kΩ range, which is the equivalent of a 2-wire resistance measurement as specified by National Instruments [13]. The PXI-2503 device switches the input to the PXI-4070 DMM between the thermistor leads. All data including cell current, cell voltage, and thermistor temperatures were recorded with *SignalExpress* every 10 s. This acquisition loop was maintained throughout the 2–3 week timeline for each run.

The feedthrough junctions were sealed at the top of the cell cap with Buna 008 O-rings. The cell was operated vented to the air through a tube, so that recombiner operation could be tested by immersing the end of the tube in water. During most runs this was not necessary, as significant electrolyte loss was not observed. Recombiner pellets consisting of platinum reduced onto alumina (*Alfa Aesar #89106*) were wedged into a groove cut into cell cap.

For most experiments, the electrolyte was 90 mL of 0.5 M LiOD made by dissolving Li metal pellets (*Sigma-Aldrich #499811*) into D_2O (99.9 atom %, *Sigma-Aldrich #151882*). For one experiment (DLER11) the electrolyte concentration was lowered to 0.1 M on the assumption that this might aid in the plating process.

The laser system employed consisted of two identical laser diode kits (*Thorlabs LTC-100B*). Each kit included a laser diode mount as well as current and temperature controllers. The laser wavelength of each diode was controlled by varying the case temperature using the supplied temperature controllers. The diodes employed varied based on the specific detuning frequencies being targeted, including Thorlabs models *HL6501MG* , *HL6750MG* and *HL6756MG* . "P" polarization was maintained for most experiments reported, as is summarized in Table 1.

2.3. Loading and resistance ratio

In accordance with procedures reported by Letts [7], electrolysis current was held at 50 mA for at least 120 h with an enclosure temperature setpoint of 15°C. For experiments DLER16B and DLER17, a stepped current protocol was used that consisted of 12+ h at 10 mA, and 4+ h each of 25, 50, 100, and 200 mA, as suggested by Coolescence LLC.

Certain experiments were performed with four additional laser welds connecting to the cathode with the purpose of measuring the resistance across the cathode using a 4-terminal AC resistance meter (*Hioki 3561*).

2.4. Data preparation

In order to use the system identification codes that fit a model differential equation to the dynamics of the calorimeter, we first interpolate all of the data onto a grid that is uniformly sampled at 10 s intervals. Although not essential, we then apply a 60 s low pass filter to the data to reduce the measurement noise. We believe that this degree of filtering is justifiable given that the calorimeter has a time constant on the order of 1800 s and as a result, for all real heat inputs, the calorimeter itself acts like a low pass filter with a time constant 30 times longer than the applied low pass filter. Nevertheless, we ran our analysis both with and without the 60 s low pass filter; the interpretation did not change.

2.5. Calibration

The main objective of calibration is to quantify the relationship between power input to the calorimeter and temperature measurements. Central to our calibration was to quantify the uncertainty in differences between measured and modeled temperature changes because these differences could be signatures of excess heat, but they could also be artifacts. We calibrated the system on a per-run basis, after loading and prior to gold plating and laser triggering, using the heat supplied by electrolytic current, i_{cell} in the absence of the laser trigger to excite the system and measure its thermal response.

The simplest model one can fit to the calorimeter's dynamic temperature measurements, $\Delta T(t)$, has one heat capacity, c and one thermal conductance, k:

$$\mathrm{d}\Delta T/\mathrm{d}t = -k\Delta T/c + Q_{\mathrm{in}}/c. \tag{1}$$

$\Delta T(t)$ is the difference between the cell temperature and the inside temperature of the enclosure containing the calorimeter. The enclosure temperature during calibration was controlled at approximately 23°C, as was earlier done by Letts [7]. The input power, $Q_{\mathrm{in}}(t)$, originates from the power applied to the cell. As is well known, an amount of

power $i_{\mathrm{cell}}v_0$ goes into splitting water into oxygen and deuterium, which is then converted back into water at the recombiner; v_0 is the thermoneutral voltage, which for deuterium is approximately 1.53 V. Letts treats this power as leaving the system without reaching the cell temperature sensors [14]. We modeled the calorimeter power according to Letts' assumption that the recombiner power escapes without affecting the temperature sensor ($Q_{\mathrm{in}}(t) = i_{\mathrm{cell}}(v_{\mathrm{cell}} - v_0)$) and also according to the "all power reaches the sensor" assumption: $Q_{\mathrm{in}}(t) = i_{\mathrm{cell}}v_{\mathrm{cell}}$. For each of the seven cathode experiments that we calibrated, the latter analysis produced a better fit with the exception of DLER7 which was not significantly different. The results reported in this document analyze the data using $Q_{\mathrm{in}}(t) = i_{\mathrm{cell}}v_{\mathrm{cell}}$

The calorimeter thermal parameters c and k were determined using the MATLAB System Identification Toolbox to fit a dynamic time series of temperature and power throughout a series of applied current transitions between 50 mA and 1.5 A that excite the thermal dynamics of the calorimeter. Data collection for the calibration phase of each experimental run took 1–2 days. Example fits to measurement data appear in Section 3. An example of fitting both with and without subtraction of the water splitting power is shown in the Linear Calibration section of the supplementary information.

2.6. Gold plating procedure

After calibration, Au plating onto the Pd surface was attempted by connecting the Au anode electrically in parallel with the Pt anode. Since this aspect of the procedure is incompletely described in Letts [7], several plating times were employed by various experiments (as low as 10 min and as high as ∼14 h, corresponding with Letts' description [9]) with some laser trials performed after each plating attempt (see Table 1). The surface was usually observed to be black at the end of the experiment after the current was switched off; during operation, the bubble sheath around the cathode made the observation of the surface difficult.

2.7. Laser triggering

After the plating step, the electrical power applied to the cell was held constant and the temperature was allowed to stabilize; this established the first part of the baseline heat rate $Q_{\mathrm{out,notrig}}$. A series of laser triggering trials was then conducted to establish triggered excess heat, $Q_{\mathrm{out,trig}}$, followed by another period without laser stimulation, which established the second baseline portion of $Q_{\mathrm{out,notrig}}$. The lasers were operated in a constant current mode, with their outputs kept to ∼10 mW each. The beams incident on the sample were kept to ∼1–2 mm in diameter, and mostly collimated over the ∼60 cm distance between the diodes and the cathode. P polarization (parallel to plane of incidence) was maintained for most experiments, in correspondence with the protocol (see Fig. 2); alternate polarization configurations were tested a few times (see Table 1). Lasers were incident on the sample generally for 40 min to 1 h at a time; however, longer time periods of up to 3–4 h were tested as well.

2.8. Excess heat and uncertainty analysis

Excess heat attributable to the laser trigger is expressed by:

$$Q_{(\mathrm{excess,trig})} = Q_{(\mathrm{out,trig})} - \underline{Q}_{(\mathrm{out,notrig})}, \tag{2}$$

where $\underline{Q}_{\mathrm{out,notrig}}$ is the averaged output power when there is no trigger applied, and $Q_{\mathrm{out,trig}}$ is the power flowing out of the calorimeter while the laser trigger is applied. In terms of temperature and conductance, k, this expression becomes:

$$Q_{\mathrm{excess,trig}} = k(\Delta T_{\mathrm{trig}} - \Delta \underline{T}_{\mathrm{notrig}}) = k(T_{\mathrm{trig,cell}} - T_{\mathrm{trig,surroundings}} - \Delta \underline{T}_{\mathrm{notrig}}). \tag{3}$$

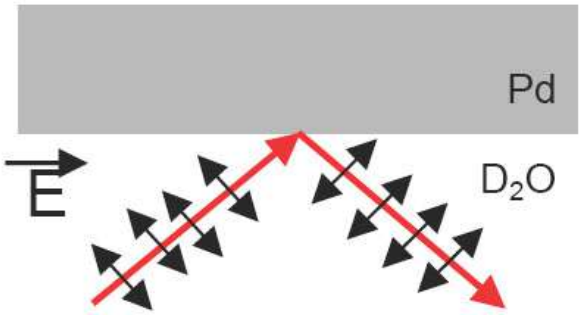

Figure 2. Schematic of "P" polarization used for most experiments.

If one assumes that the sources of uncertainty are uncorrelated, then the uncertainty associated with this computation, $\sigma_{Q\text{excess,trig}}$, is the 2-norm of the individual uncertainties:

$$\sigma_{\text{Qexcess,trig}} = \sqrt{\sigma_1^2 + \sigma_2^2 + \sigma_3^2 + \sigma_4^2}, \tag{4}$$

where

$\sigma_1 = \sigma_k \left| \langle\, T_{\text{trig,cell}} - T_{\text{trig,surroundings}} - \Delta T_{\text{notrig}} \,\rangle_t \right|$ uncertainty in thermal conductance,

$\sigma_2 = k\sigma_{T_{\text{trig,cell}}}$ cell temperature variance during triger,

$\sigma_3 = k\sigma_{T_{\text{trig,surroundings}}}$ surroundings temperature variance during triger,

$\sigma_4 = k\sigma_{\Delta T_{\text{notrig}}}$ untriggered baseline temperature variance.

σ_k is the uncertainty in thermal conductance determined from the calorimeter calibration, and $\langle\,\rangle_t$ denotes a time averaged quantity. Note that this uncertainty estimate is not the most conservative. If we make no assumption about the correlation, then the total uncertainty is bounded by the 1-norm of the four uncertainties above:

$$\sigma_{Q\text{excess,bound}} \leq \sigma_1 + \sigma_2 + \sigma_3 + \sigma_4. \tag{5}$$

Typically the largest source of uncertainty is in σ_4, the establishment of a stable baseline before and after the application of the laser trigger as will be discussed in Section 3.

It is worth noting that the uncertainty analysis that we apply herein differs from that practiced by Hagelstein and Letts. They used the goodness-of-fit to an exponential relaxation time to model the triggered temperature rise in order to estimate the uncertainty of their excess power observations. Also, it is notable that the error bars on our results in Fig. 9 are larger than those in the comparable work by Hagelstein and Letts [17]. Details of the method used by Hagelstein and Letts were not provided; however, we make three observations: (1) typically, we see no triggered temperature rise, which makes use of the Hagelstein-Letts technique problematic. (2) The relaxation time model used by Hagelstein and Letts presumed that excess heat signatures appeared as a step change in the calorimeter. While this presumption may be appropriate for their dataset, that is not the case in the present work. (3) The detailed uncertainty estimation methods used by Hagelstein and Letts are not included in their publication. It is possible that some uncertainties in both the thermal parameters and the temperature measurements may not be fully accounted for in the Hagelstein Letts uncertainty estimation method.

Table 1. Summary of experiments discussed in this manuscript.

Cathode run	LiOD conc. (M)	Plating times (h:min) Sequence 1	Sequence 2	Sequence 3	Approx. mag. field (G)	Polarization pairs tested*
DLER5	0.497	0:10	0:55	4:55	200	PP & PS
DLER6	0.509	2:10	4:04	5:58	200	PP & PS
DLER7	0.519	2:04	3:56	14:35	200	PP
DLER8	0.5	6:19	4:40		200	PP
DLER10	0.446	2:00	6:18		200–500†	PP
DLER11	0.1	2:20			500	PP
DLER14	0.5	2:00			500	PP
DLER16B	0.5	6:43			500	PP
DLER17	0.5	8:21			500	PP

*Each letter corresponds to the polarization of light from a particular diode, P or S, corresponding to parallel and perpendicular to the plane of incidence respectively.
†Magnetic field was 200 G for loading phase, 500 G for laser experiments.

3. Results

In an attempt to demonstrate the open access to both experimental methods and raw data that is necessary for collegial and conclusory scientific progress, the raw data for the experiments in Table 1 and discussed below are available *here*.

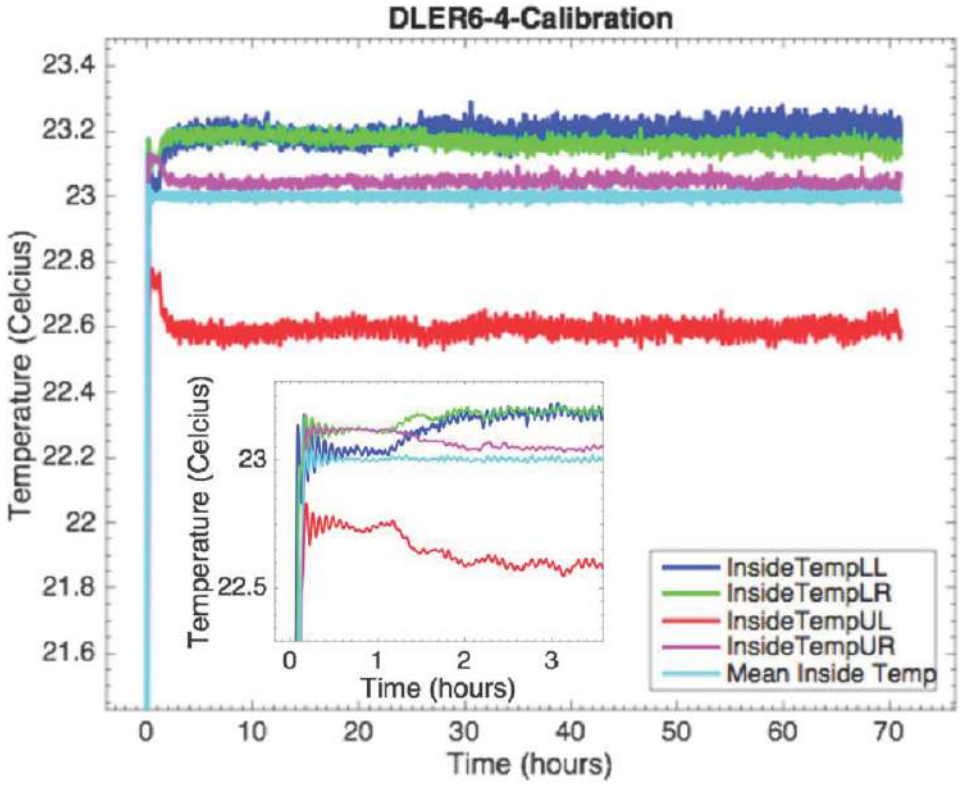

Figure 3. Typical enclosure temperature stability. Inset shows early time stabilization period.

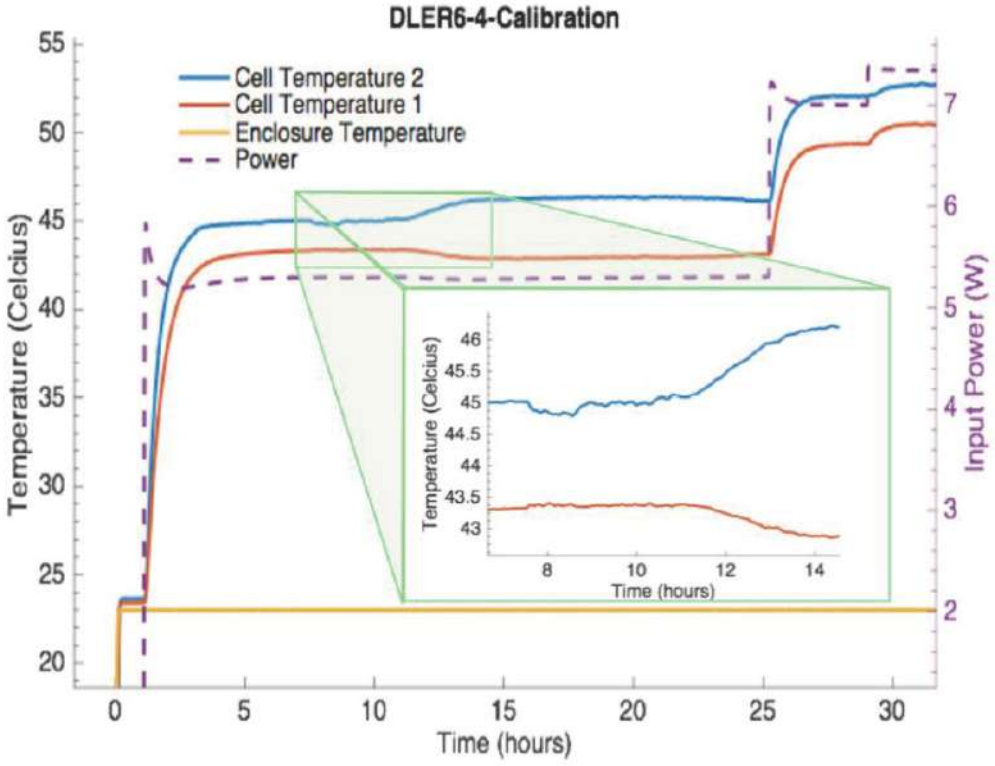

Figure 4. Example of anti-correlated electrolyte temperature sensing instability occurring during calibration period. Inset focuses on time period where instability occurs.

3.1. Materials preparation

The materials preparation end-points specified by Letts in his published works consist primarily of visual descriptions of the resulting surface after polishing, annealing, and etching. These were generally achieved in the present work. However, due to the inability to visually determine properties such as surface r.m.s. roughness, surface-based impurity concentration, oxide thickness after etching, or other potentially relevant material parameters, it is unclear whether our produced material matched that obtained by Letts in the original work by quantitative measures.

3.2. Enclosure temperature

Maintaining a constant enclosure temperature was essential for the calorimetry practiced in this experiment. A representative example of temperature measurements over a 70 h run is shown in Fig. 3.

The abbreviations LL, LR, UL, and UR refer to lower left, lower right upper left and upper right locations in the enclosure respectively. This dataset, which was typical, illustrated a number of important details. As shown in the inset, we saw that the control loop that stabilizes the enclosure temperature leveled out after several hours. Although likely adequate for this experiment, there remained a small oscillation at about 3.5 mHz (∼5 min period) which was undesirably close to the roughly 25 min thermal relaxation time of the calorimeter. Assuming that the source of these

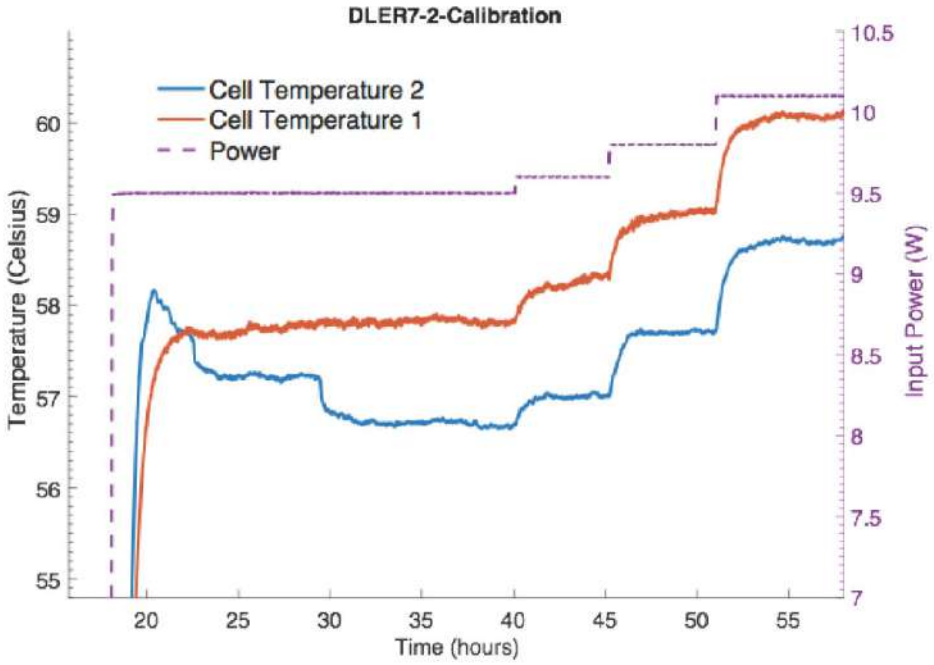

Figure 5. Example of single-thermistor temperature sensing instability.

fluctuations was the software-based PID loop controlling the enclosure temperature, a more judicious choice of the proportional, integral and derivative gain parameters might have eliminated the oscillation.

The four measurements agreed to within 0.8°C when in equilibrium. The sensor data had a noise amplitude of on the order of 0.2°C; The apparent increase in sensor noise at hour 25 correlated with an increase in applied cell power. The sensor noise appeared to not be completely correlated because the mean enclosure temperature was less noisy than the individually measured temperatures. Based on these findings, we used the time varying mean of all of the enclosure temperature measurements for data analysis purposes.

3.3. Electrolyte temperature sensing instability

All experiments analyzed showed evidence of temperature sensing instability. Such instability interfered directly with attempts to interpret temperature changes as anomalous heat. A representative example in Fig. 4 shows thermistor and power measurements before, during and after a plateau in applied power.

Between hour 10 and hour 15, while the input power and enclosure temperature were relatively stable, the two cell temperature measurements were not stable; they shifted *in opposite directions*. One plausible explanation is that the cap that holds the glass tubes containing both thermistors was tilting and causing thermistor 1 to move further from the electrodes and thermistor 2 to move closer to them. We note that the cap had an o-ring seal that was press-fit into the glass beaker. The magnitude of the temperature shift was about 0.5 and 1.2°C for the first and second sensors, respectively.

Other observations of cell temperature sensing instability suggest that individual thermistors might have shifted position in the electrolyte during the runs, as shown in Fig. 5. In this example, between hours 19 and 40, under

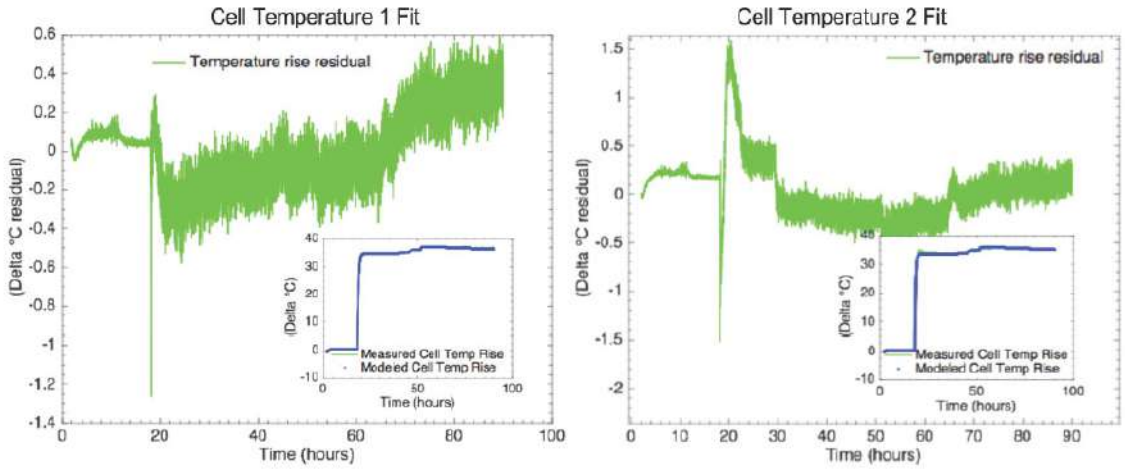

Figure 6. Model fits to the two cell temperature readings obtained during run DLER7-2. Delta (°C) corresponds to temperature difference between cell and enclosure.

constant applied power, the first thermistor rose monotonically as expected while the second thermistor fell about 1.5°C in several steps.

3.4. Calorimeter calibration observations

When the ordinary differential equation described in Section 2.5 was applied to calibration data we obtained values for the calorimeter's lumped parameter heat capacity,c, and thermal conductance, k, as well as the standard deviations for these parameters. The thermal conductance in particular was essential for the analysis of the laser trigger experiment because the input power during that experiment was held constant, and in steady state, the temperature rise of the calorimeter is $k\Delta T$.

Figure 6 shows the residual, $e_T = \Delta T_{\text{measured}} - \Delta T_{\text{modeled}}$, of the fit to cell temperatures 1 and 2 measured during run DLER7-2 (cathode run DLER7, data set 2), a portion of which is shown in Fig. 5. The insets of each plot show the measured and modeled temperatures overlaid, illustrating the importance of viewing residuals to assess the fit. The input data used for the fit is the power time series, $i_{\text{cell}}v_{\text{cell}}$. As expected, we obtained a better fit using cell temperature 1, which appeared to be more stable, particularly between hours 20 and 40 (note differences in scale). For each experimental run, we determined which sensor was more reliable based on the fit to the model. This sensor, 1 in the example provided, was used for analyzing the laser trigger experiments.

The difference between modeled and measured temperature provided an indication of calorimeter accuracy. The product ke_T of the temperature residual, e_T, and the thermal conductance during calibration is a direct measure of anomalous heat that arises from artifacts (mechanical, electrical, etc.) during calibration and is an indication of heat artifacts that could have arisen during experimentation. In all nine runs, we kept track of the largest heat artifacts that arose during each calibration; these ranged in magnitude from 0.13 to 0.46 W. Many of these artifacts appeared as brief disturbances to the thermometry during changes to the input power.

3.5. Attempts at excess heat observations

A representative time series of enclosure and cell temperatures and applied power is shown in Fig. 7. Triangles indicate the times at which laser triggers were applied, altered to a new difference frequency, and ended. The time series, which is over 70 h long, includes measurements on two separate days.

Figure 8 shows instantaneous excess heat measurements inferred from the temperature changes relative to the average baseline temperatures (plotted in gray) prior to and after each series of laser triggers. Each color change (blue, red, green, cyan, and magenta) indicates the application of a new difference frequency to the cathode. The horizontal bars above and below the excess heat measurements represent one standard deviation on the excess heat measurement at each laser difference frequency.

The laser power input was not observed, as it tended to be below the noise floor. The results of the laser trials of experiment DLER7-3 are summarized in Table 2. In both laser trial series, we observed that the excess heat rate baselines before and after the laser trials differed by 10's of mW. We attribute this to calorimeter drift, as referenced previously.

By far, the largest contribution to the excess heat measurement uncertainty is σ_4, the untriggered baseline temperature variance; this uncertainty ranged from about 15 to 21 mW. Clearly, a priority for any redesign of this experiment would be to stabilize the temperature measurements to establish a more accurate baseline. The next largest source of error is σ_2, cell temperature variance during trigger. This uncertainty contribution was as large as 18 mW. Note that we did not see evidence of an exponential rise upon triggering as reported in reference [7]. Had we observed such an exponential rise, this uncertainty term would have been modified by an accounting for an exponential fit to the output power. The next largest source of uncertainty is σ_3, the surroundings temperature variance during the trigger; this uncertainty contribution ranged up to about 8 mW. The smallest uncertainty contribution was from the uncertainty in the thermal conductance out of the calorimeter determined from the calibration of the calorimeter. This further illustrates

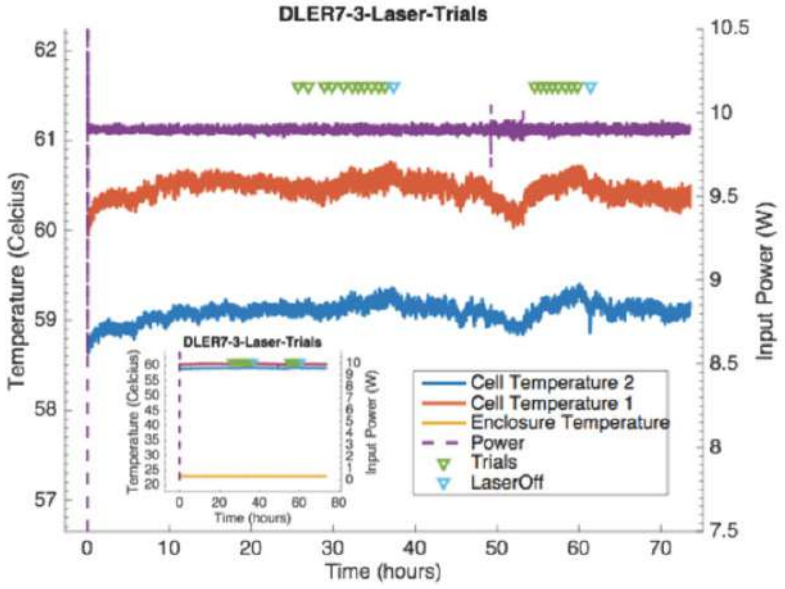

Figure 7. Representative laser trial data taken over a period of several days for experiment DLER7-3.

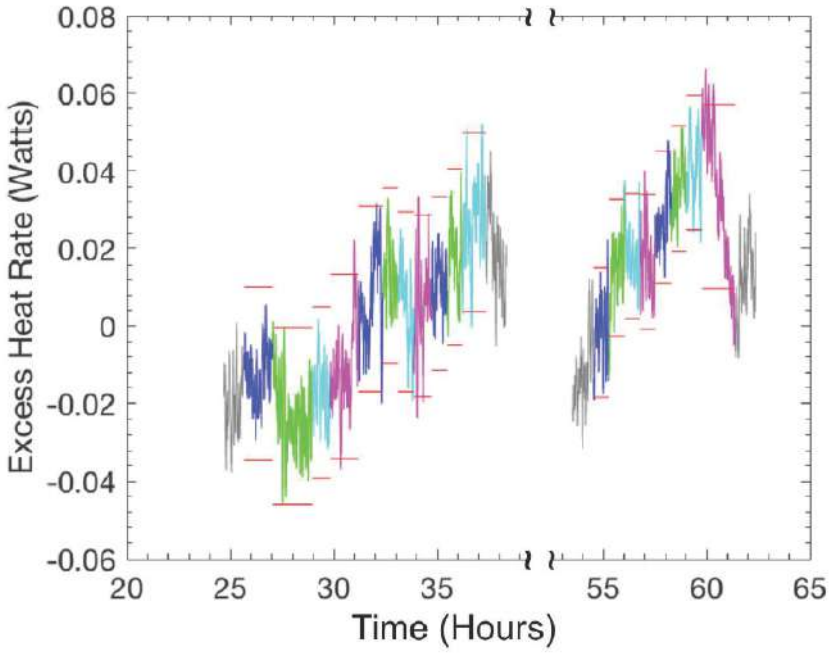

Figure 8. Calorimetric data analysis from Fig. 7, showing excess heat rate estimates including error bars. The figure depicts two separate dual-laser trials done over the course of two days. The gray plot portions bounding each trial are heat rate *without* laser irradiation. Different colors correspond to difference laser detuning frequencies. Red bars above and below the lines represent one standard deviation.

how a triggered excess heat experiment such as this is not very sensitive to the calibration method and is primarily affected by sensor stability.

A summary of excess heat rate as a function of difference frequency for all 231 laser triggered trials across nine cathode runs is shown in Fig. 9.

A rudimentary estimate of the average excess heat measured across all of the runs, and its uncertainty was obtained by averaging all the data and taking as the uncertainty the standard deviation of the excess heat measured during each laser trial. By this measure, the laser trials indicated an excess heat of 6.1 $\pm$ 21.6 mW. For comparison, the measurements reported in [7] are also shown in Fig. 9. Both datasets provided error bars on the measurements; however, as discussed in the methods section, the uncertainty analysis methods differ.

A histogram of the excess heat results measured at each laser triggered trial is shown in Fig. 10. We see that there is a very slight positive heat rate measurement of about 6 mW. It is possible that this is caused by the absorption of power from the laser trigger, although this is below the resolution of any one excess heat rate measurement.

Figures 9A and 10 show occasional observations approaching 100 mW of heat rate excess and heat rate deficit. It is worth noting that the largest magnitude heat rate observations are also those with the greatest measurement uncertainty. This phenomenon is depicted in Fig. 11. The slope of uncertainty vs. measurement is close to unity.

3.6. Resistance ratio measurements

Most of the attempts at resistance ratio measurements were met with experimental difficulty, making interpretation difficult. However, during run DLER17 the cathode was observed to achieve a resistance ratio (R/R) of 1.8, corre-

Table 2. Excess heat and uncertainty contributions calculated from run DLER7-3 (cathode run DLER7, data set 3).

Day	Trial	Frequency (THz)	Q_{excess} (W)	σ (W)	σ_1 (W)	σ_2 (W)	σ_3 (W)	σ_4 (W)
1	1	16.4	−0.012236	0.022379	0	0.006073	0.004456	0.021073
1	2	15.3	−0.023286	0.02285	0.000001	0.007163	0.005171	0.021073
1	3	14.5	−0.017147	0.02215	0.000001	0.005053	0.004585	0.021073
1	4	14.7	−0.010404	0.02383	0	0.009794	0.005278	0.021073
1	5	14.9	0.006955	0.023973	0	0.010341	0.004867	0.021073
1	6	15.1	0.012993	0.022735	0.000001	0.006131	0.005932	0.021073
1	7	15.3	0.006209	0.023202	0	0.008303	0.005033	0.021073
1	8	15.5	0.005101	0.023468	0	0.006869	0.007712	0.021073
1	9	15.7	0.010849	0.02237	0	0.005992	0.004518	0.021073
1	10	15.9	0.017819	0.022779	0.000001	0.007875	0.003573	0.021073
1	11	16.1	0.026829	0.023088	0.000001	0.00824	0.004591	0.021073
2	1	16.1	−0.001708	0.016825	0	0.005722	0.005195	0.014944
2	2	15.9	0.015012	0.017669	0.000001	0.008192	0.004662	0.014944
2	3	15.7	0.01806	0.016134	0.000001	0.004712	0.003842	0.014944
2	4	15.5	0.016601	0.017393	0.000001	0.006902	0.005616	0.014944
2	5	15.3	0.028174	0.017008	0.000001	0.006653	0.004654	0.014944
2	6	15.1	0.035451	0.01629	0.000001	0.005809	0.002881	0.014944
2	7	14.9	0.041971	0.017325	0.000002	0.00739	0.00471	0.014944
2	8	14.7	0.033394	0.023625	0.000001	0.017832	0.004103	0.014944

sponding to a D/Pd loading of ∼0.9.

4. Discussion

4.1. Impediments to replication

An objective of this experiment was to faithfully replicate the DLE as practiced by Letts. Given the importance of Letts' claims to the low energy nuclear reactions community, we recommend an in-person collaboration with him for those replicating his work. We estimate that it would take 2 months of his time to facilitate a definitive outcome.

It is worth noting that the DLE, if verified, represents a power source (up to 300 mW) that is approximately up to 4% of the applied electrical power (∼8 W). An effect of that scale has no immediate technological value as an energy source, even if an inexpensive source of Pd could be found. However, the scientific value of replication would be significant, given that such an effect is considered highly improbable by much of the physics community.

4.2. Apparatus replication fidelity

The make and model of much of the commercially available equipment, and the mechanical drawings for custom parts, used in our apparatus were either identical to Letts' original apparatus or altered with Letts' approval. We can therefore make some claims about the performance of the apparatus, and comment on the observation differences between ours and Letts' original experiment.

4.3. The importance of calibration method

A common calibration practice is to take several points from the steady state plateaus of temperature vs. power and produce a linear fit. While this approach provides a measure of calorimeter sensitivity in W/°C [15] we submit that this approach is inadequate for the purpose of establishing a calorimeter's propensity for heat artifacts. As shown in

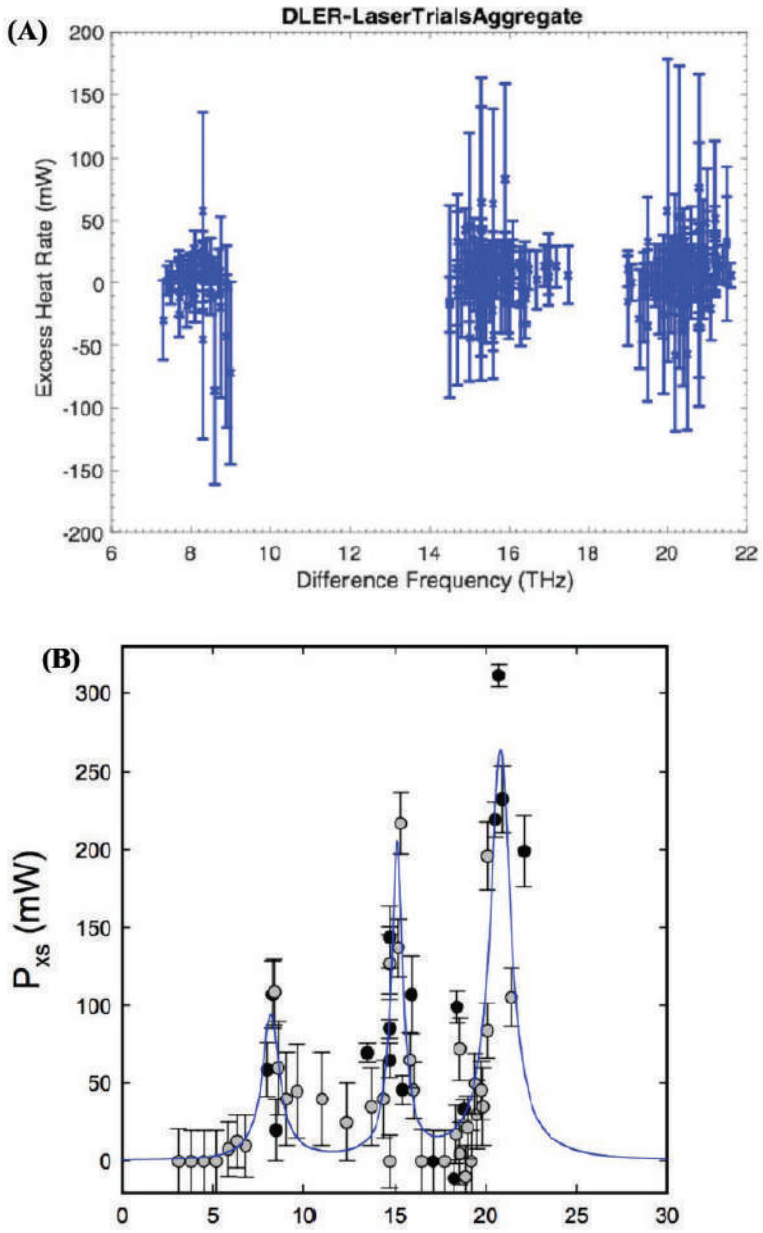

Figure 9. (A) Aggregated calorimetric data obtained for all laser triggered trials discussed in this study. Error bars are 1 sigma standard deviations. (B) Letts' reports of excess heat as a function of detuning [7].

Fig. 6, a dynamic model fit to all of the data from a multi-day calibration run provides a more complete indication of the size of heat artifacts and the conditions where they occur.

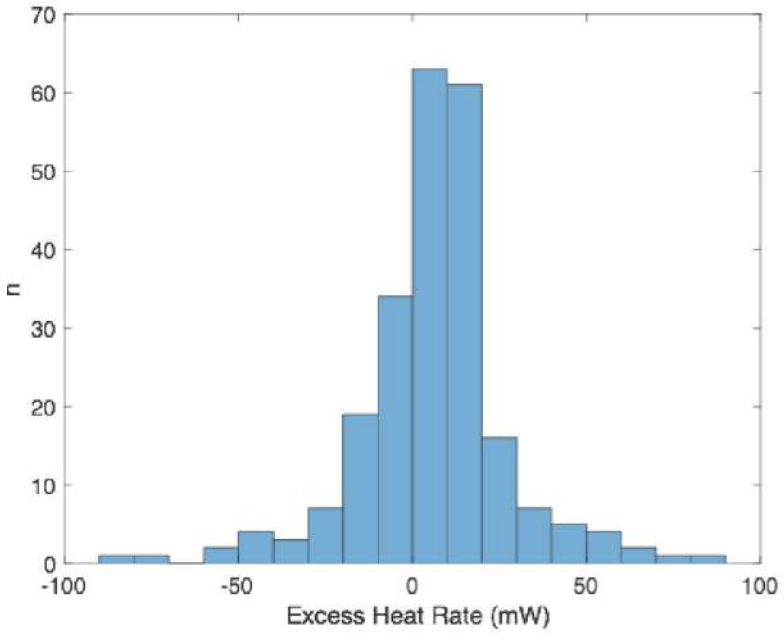

Figure 10. Histogram of all 231 laser triggered trial excess heat measurements.

Our data analysis differs in significant ways from data analysis [16] of the original DLE, for example Eq. (1) in this report is equivalent to the modeling of the calorimeter's relaxation time; however, what is different is our application of system identification to the complete calibration dataset instead of selected portions, and the examination of residuals. This procedure revealed myriad artifacts that one would typically address before attempting to detect excess heat, as discussed below. As discussed in the Supplemental Information, the quality of the fit using system identification tools did not find support for the assumption in [7] Eq. (2) that the power applied for water splitting can simply be subtracted from the input power. This suggests to us that heat from the recombiner is traveling into the electrolyte. Nevertheless, whether or not one analyzes the data using $Q_{\rm in}(t) = i_{\rm cell}(v_{\rm cell} - v_0)$ or $Q_{\rm in}(t) = i_{\rm cell}v_{\rm cell}$, this paper's overall conclusion regarding the observation of excess heat, and its uncertainty does not change appreciably. The two calibration methods produce two values for the thermal conductivity, k, to the surroundings that differ by about 30%; however, due to the differential nature of this triggered experiment, this results in a simple scaling of the result and would not cause a failure to observe excess heat were it present. The effect on the uncertainty is also scaled, as is readily observed inspection of the terms in the uncertainty analysis. For completeness, we ran all calibrations and analyses with $Q_{\rm in}(t) = i_{\rm cell}(v_{\rm cell} - v_0)$; instead of an excess heat result of 6.1 $\pm$ 21.6 mW, we obtained 4.6 $\pm$ 16.2 mW.

4.4. Temperature sensing artifacts

An important finding from the replicated apparatus is its inherent temperature sensing artifacts that produce artifactual signatures of excess heat. Our calibrations showed that the thermal conductance out of the calorimeter is about 270 mW/°C. We saw temperature shift artifacts that could be attributed to mechanical instability of the calorimeter cap that ranged from 0.5 to 1.2°C; artifacts this large correspond to heat artifacts on the order of 135–324 mW. It is worth

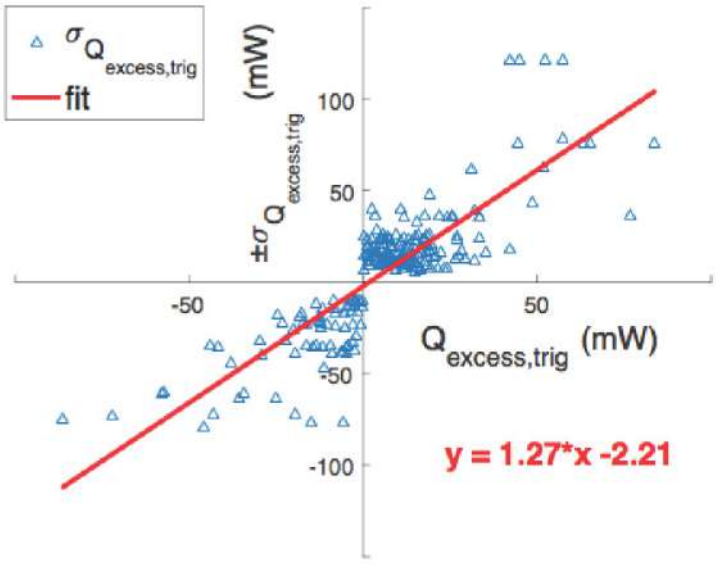

Figure 11. Uncertainty in excess heat rate (signed) vs. excess heat rate.

noting that such artifacts are on the same order or larger than the excess heat observations reported in Letts' original experiment. It is hard to predict whether or when spurious movements of the thermistors will occur during any given attempt to trigger an excess heat effect; however, any credible claim of excess heat caused by an applied laser trigger should necessarily be done on an apparatus with demonstrably stable temperature sensing. One potential way to improve the temperature sensing stability would be to clamp the calorimeter cap in place and to ensure that all sensor mounts are supported at multiple points.

An additional potential source of spurious "excess" heat is variable recombiner function. Since the operating temperature of the experiment spans a range of ∼40°C and the behavior of the recombiner, as with any catalyst, should be expected to vary significantly with temperature, sudden exothermic bursts might be observed when recombiner pellets activate. Considering that our analysis shows the recombiner heat to be poorly separated from the electrolyte, care should be taken when interpreting excess heat events occurring during or shortly after major changes in cell temperature.

Not all of the temperature sensing artifacts observed by us could be explained by motion of the cell cap. For example, in Fig. 5, sensor 2 was observed to produce artifacts independently of sensor 1. This may be an indication of mechanical or electrical problems affecting only sensor 2. A 1.5°C artifact like the one shown above in Fig. 4 corresponds to a heat rate artifact of about 400 mW. With artifacts this large the calorimeter may not be well suited for precision calorimetry. The DLE attempts to trigger an excess heat event while running the calorimeter at constant power after a days-long phase comprising loading and plating. It was standard procedure to let the calorimeter stabilize at constant input power before applying the laser trigger. However, this can not guarantee that heat rate artifacts will not occur coincident with the laser trigger.

Given that the excess heat effect reported by Letts is up to a 4% effect (up to 300 mW out of 8 W), the calorimeter used to investigate such an effect would ideally be designed and confirmed to have no heat rate artifacts greater than about 10 mW. The authors believe that this is feasible; however, it would require a careful redesign of the calorimeter.

Electrical noise on the temperature sensors might also need to be reduced.

4.5. Electrolyte temperature non-uniformity

In one report of the DLE [17], the discrepancy between cell temperatures is said to be about 0.1°C or less; in our replication attempt, the discrepancy between the two cell temperature sensors was 20–30 times larger. Given the faithful replication of the parts used in this experiment, we find this difference noteworthy. Our observations spanning over four months of experiments show that the replicated apparatus has temperature differences within the electrolyte that span at least several °C. Neither our experiment, nor the Letts' original experiment stirred the electrolyte.

4.6. Venting

The original design of this experiment was vented to air through a small vent tube. The intent of this tube was to allow gas to escape when the recombiner was not functioning properly. In the original work, the method of submerging the exit-end of the tube in liquid was used to check for recombiner failure which would be expressed as bubbling. A concern with this approach is that a system open to air may take up and substitute light water for heavy water. Proton contamination, as this is called, has been raised as a possible failure mechanism because it is claimed [18] that hydrogen will go into Pd preferentially to deuterium.

4.7. Gold plating

In both the JCMNS 2010 as well as personal communication, Letts does not specify a particular plating time. The Current Science publication specifies plating in 10 min increments until the effect is observed. 10 min plating sequences were utilized early on in the experimental campaign (see Table 1), however, since no effect was observed, and with the guidance of the previous single laser work in which significantly longer plating times were employed, sequences as long as 14 h + were attempted. Bubbling and color change on the Au anode (from gold to red to black) over the course of a few hours were consistently observed during the plating process.

The resulting Au deposit in the original work is characterized only by its visual appearance. We replicated the Letts plating method which places the Pt and Au anodes in parallel with each other. A ramification of this is that the sum, but not the division, of current between the two anodes is unknown; this complicates our ability to know how much Au might have been applied to the cathode by Letts, and also how much plating may be occurring in our experiments. A suggested approach would sense current flowing from both anodes.

4.8. Heat measurements

Within the range of experimental uncertainty, the 231 excess heat measurements at each difference frequency were consistent with no excess heat triggered by the dual-laser stimulation. While it is impossible to disprove the claims of the Letts' original DLE, this work does refute the claim that results are highly reproducible [8] The quantity of laser triggered trials analyzed is 231 across 9 cathode runs, exceeding what is reported in the Letts' original DLE [7]

One question that might arise is whether each laser trial was of sufficient duration to trigger and sense an excess heat effect. We note that each dual-laser trigger was applied for a time longer than the thermal time constant, c/k, of the calorimeter which is about 30 min. Letts reported an excess heat response that is observed as rapidly as $\sim$5 min after laser triggering [7]

While outliers of 90 mW excess or absorbed heat were observed, these measurements had the least certainty. The excess heat measurements with the greatest certainty (smallest uncertainty) had the smallest magnitude of excess heat

rate (whether positive or negative). This trend is shown in Fig. 11. A validation of any cold fusion effect will need to show that the measured effect persists as the uncertainty of measurements is reduced; in this work, that was not observed.

5. Conclusions

In this work we attempted a high-fidelity replication of claims of excess heat triggered by dual-laser stimulation in an electrochemical system of palladium deuteride. We employed and described calorimeter calibration and error analysis methods that we believe are appropriate and adequate to the experimental objective. Despite having replicated Letts' original experimental design and protocol to the best of our ability, and conducting 231 attempts across 9 cathode runs, we did not observe evidence of laser-triggered excess heat events on the order of 100 mW reported by Letts. The average excess heat rate observed from all runs was 6.1 ± 21.6 mW with $\sim$10 W of input electrical power.

However, several issues hampered our ability to replicate the work, including limited engagement with Letts (the author of the original DLE), the inability to directly compare material parameters of our cathodes with "successful" cathodes, and spurious calorimetric fluctuations due to apparatus design issues.

Dennis Letts claims that his results are highly reproducible [8]. We recommend that any future replication attempts provide for direct collaboration with Letts on a redesigned experimental apparatus.

Supplemental Information

S1. Calorimeter Temperature Control Hardware

Temperature-controlled enclosure consists of an *Edgestar 84* can beverage cooler with all but the bottom-most rack removed. Since the enclosure will only cool the system, a feedback mechanism needs to be established to provide heating to achieve a given setpoint.

The general principle of the temperature control design is to circulate mixed (hot and cold) air from the back of the enclosure up towards the top, down the front glass panel and then back towards the mixing area. The general schematic is shown in Fig. 12, an interpretation of Letts' original designs:

Two 12 V *CoolerMaster SickleFlow* 120's are used. Their activation switch is a solid state relay connected to a 12 V power supply and the NI DAQ (see below). The two fans are strapped together with twist-ties. A nichrome heating wire wrapped in a coil is connected by screws to two holes on opposite ends of the fan bank. Power for this heater is supplied by one of the two *E3632A* power supplies in the setup.

The back of the enclosure showing the cold wall built into the cooler, the two 12 V fans, and (barely visible above the fans) the heating wire is shown in Fig. 13.

The air distribution system consists of several pieces of custom-cut insulation board, with four additional 2 inch fans guiding the air up towards the enclosure roof.

Back and angled views of the air distributor are shown in Fig. 14. The bank of fans, which sits on top of the open portion of the air distributor in the right photo (Fig. 14) is shown in Fig. 15.

Each fan has a hole cut in the bottom (not pictured). These fans are powered on the same circuit that powers the two larger fans along the back wall, and the entire system is left on for the duration of the measurement.

S2. Cell

S2.1 Body

A picture of assembled cell inside the calorimeter is shown in Fig. 16.

The cell body is a *Kimble-Chase tall form Berzelius Beaker*.

S2.2 Thermistor probes

The thermistor probes are made as follows: *Flint glass tubes* are melted shut at one end, into which are placed thermistors that have had their leads soldered onto twisted pairs taken from Ethernet cables (see *this guide* for a description of the procedure). Electrical or Teflon tape is used to prevent the wires and solder blobs from contacting each other and shorting the probe. Shorts are clearly noticeable during the experiment as the apparent temperature spikes to clearly unreasonable values (hundreds of °C).

S2.3 Cell lid

Designs given by *Dennis Letts* have been used as a starting point to fabricate the cell lid. However, it was discovered that the slots into which the recombiner pellets are supposed to sit (lowest groove pictured above) are too thin at the specified width of 0.0625". When doubled, the groove allowed for a good press fit.

S3. Final Washes

The following final sample washes were applied to the cathode before the experiment began:

DLER5: (Not recorded),
DLER6: Sonicated for ∼15 min in 1:1 H_2O:IPA in cell body. Washed in copious amounts of distilled water, then dried with N_2. Left to dry completely overnight,
DLER7: None (used as received from Letts),
DLER8: Sonicated 30 min with Cole-Parmer compound remover solution, dried with N_2,

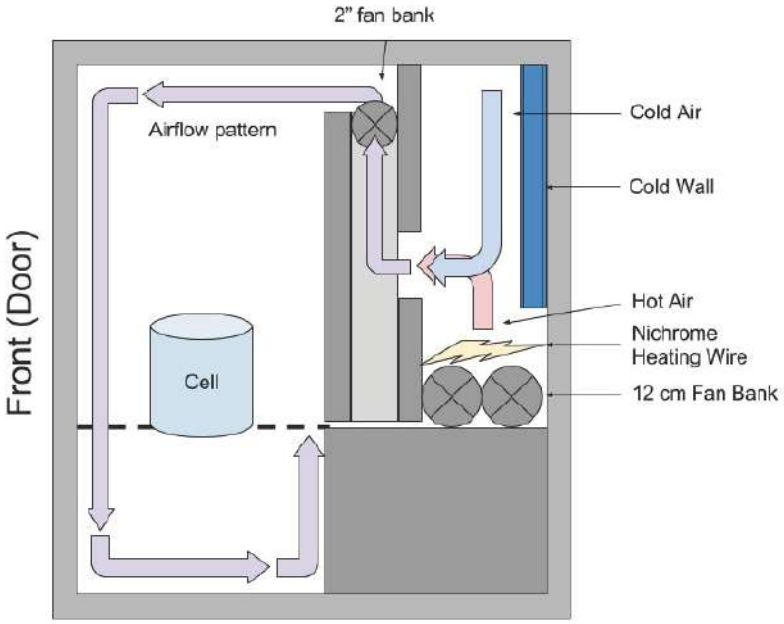

Figure 12. A schematic of the temperature-controlled enclosure.

Figure 13. The back of the enclosure showing the cold wall built into the cooler, the two 12 V fans, and (barely visible above the fans) the heating wire.

DLER10: Cathode washed with acetone before start of experiment,
DLER11: Sonicated with Cole Parmer compound remover 30 min, air-dried.

S4. Model Fitting to Calibration Data

4.1. Linear calibration

The calibration (Fig. 17) is typical of that obtained by fitting the steady-state response of the calorimeter to the input power at various steps. It is presented for comparison to the calibration obtained by the full system identification model. The inverse slope for Cell Temp1 is 0.267 W/°C which is in close agreement with the thermal resistance parameter from system identification. What is missing from a fit to only several plateau data points are all of the artifacts stemming from apparatus instabilities.

As an example of dynamic model fitting to calibration data, and some of the models that we tried, we illustrate our calibration results for Cathode DLER10. Figure 18 is the full calibration dataset for input power and measured temperatures.

Notice that the full dataset includes about 0.5 h of initial data taken before the enclosure temperature stabilized to

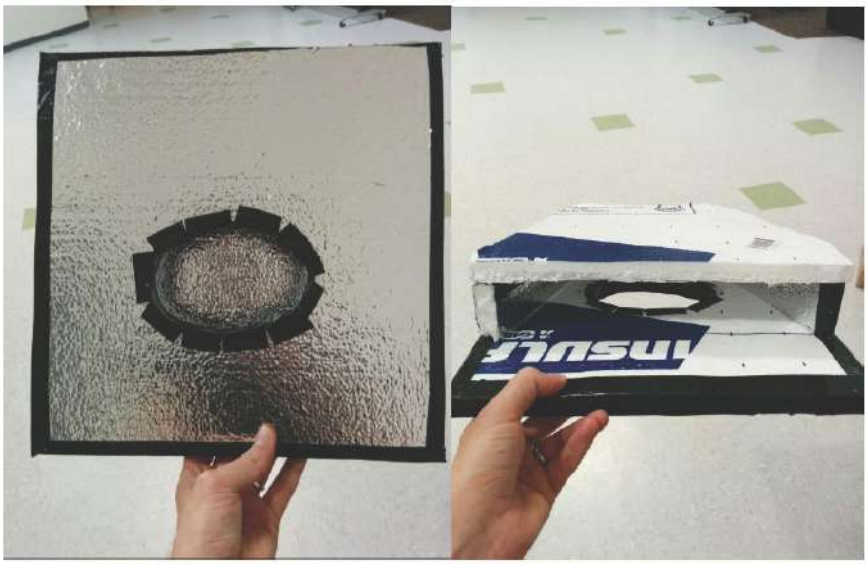

Figure 14. The custom-built air distributor, viewed from the back (left image) and top (right image) as viewed from the front of the enclosure.

about 23°C. As the calorimetry is isoperibolic, this portion of the data are excluded from the calibration. Notice also that Cell Temperature 2 is not stable. As discussed in the manuscript, Cell Temperature 1 was used. First, we show the result of applying the linear heat transport model

$$\mathrm{d}\Delta T/\mathrm{d}t = -k\Delta T/c + i_{\mathrm{cell}}v_{\mathrm{cell}}/c.$$

where ΔT is the difference between Cell Temperature 1 and the Enclosure Temperature, $i_{\mathrm{cell}}v_{\mathrm{cell}}$ is the electrical power fed into the cell, and k and c are fits to the calorimeter's thermal conductance and heat capacity respectively. This first model makes the assumption that power that gets converted into chemical energy by splitting water and is then released at heat in the recombiner exits through the calorimeter through largely the same path as the rest of the power that simply appears as direct heating of the electrodes and electrolyte. This first model also makes the

Figure 15. The bank of fans, which sit on top of the open portion of the air distributor as shown in the right image in Fig. 14.

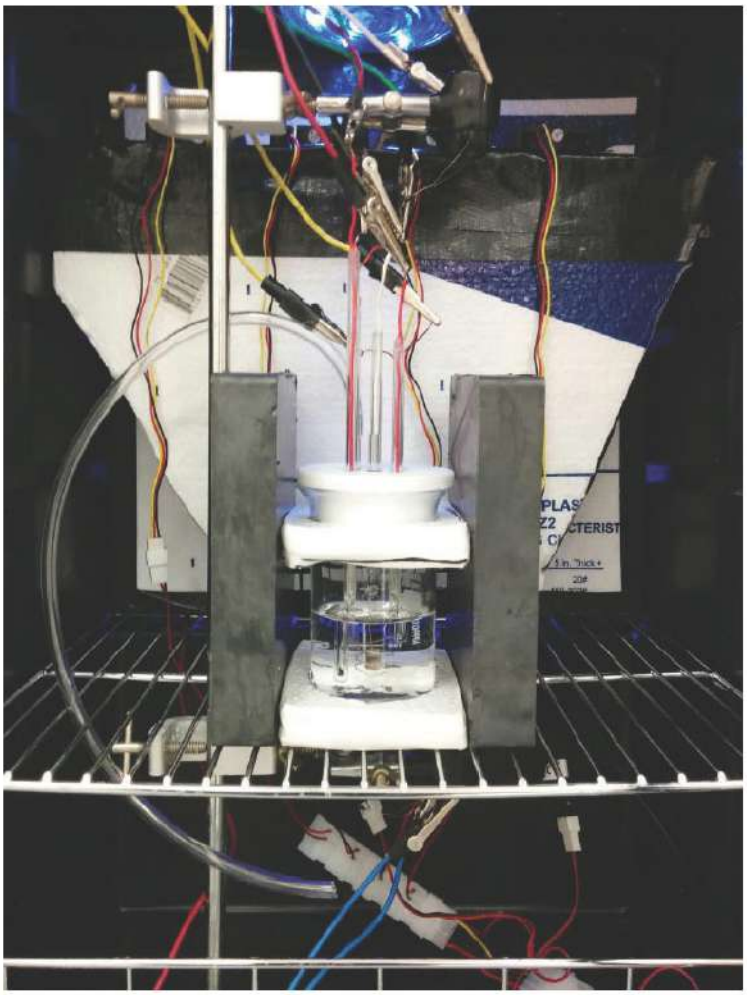

Figure 16. A picture of assembled cell inside the calorimeter, as would be present during a typical experimental run.

assumption, consistent with the assumption of Letts, that heat was removed by first order processes (conduction and convection). Figure 19 shows the measured and modeled cell temperature difference time series. The model was fit using the Matlab System Identification Toolbox's grey box model routine greyest.

Notice from Fig. 19 that this first model underestimates the cell temperature rise for small power inputs and overestimates the cell temperature rise for high power inputs. In spite of the model's simplicity, it explains the data fairly well, with a normalized root mean square error of only 4%.

S4.2 Linear calibration with subtracted electrolysis power

Next, we apply the assumption that power that goes into electrolyzing water gets carried away by the rising bubbles in the electrolyte, and thereafter, because the recombiner is somewhat removed from the electrolyte, that power does not

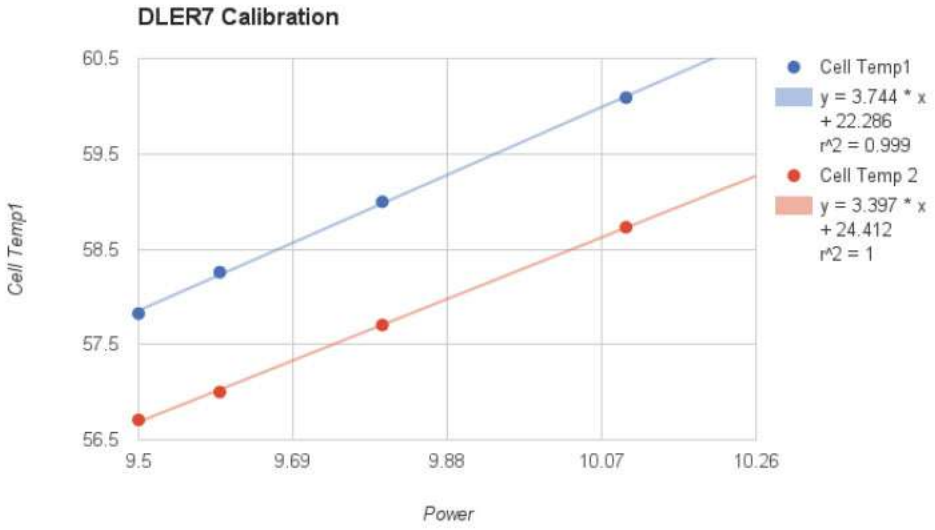

Figure 17. A typical calibration obtained by fitting the steady-state response of the calorimeter to the input power at various steps.

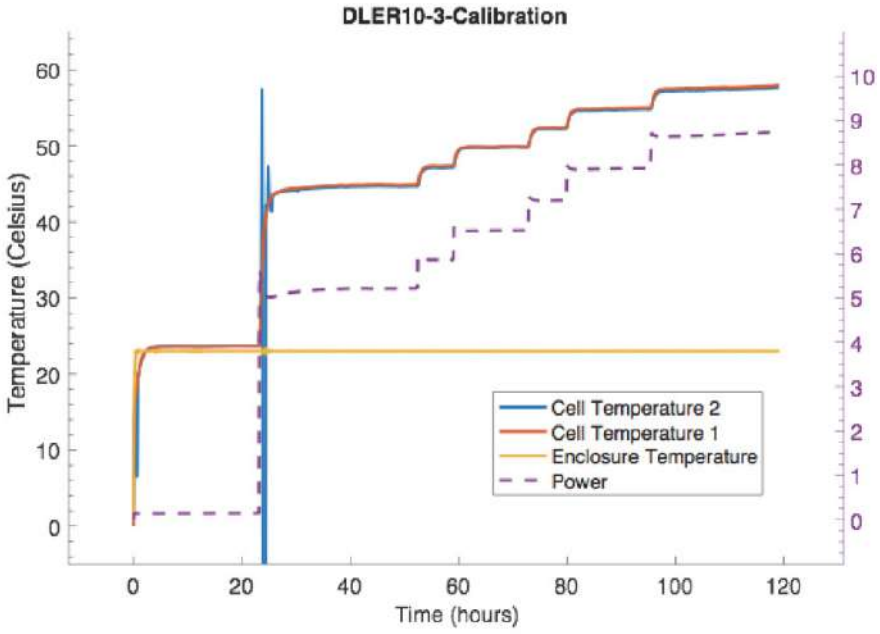

Figure 18. Full calibration data set for input power and measured temperatures.

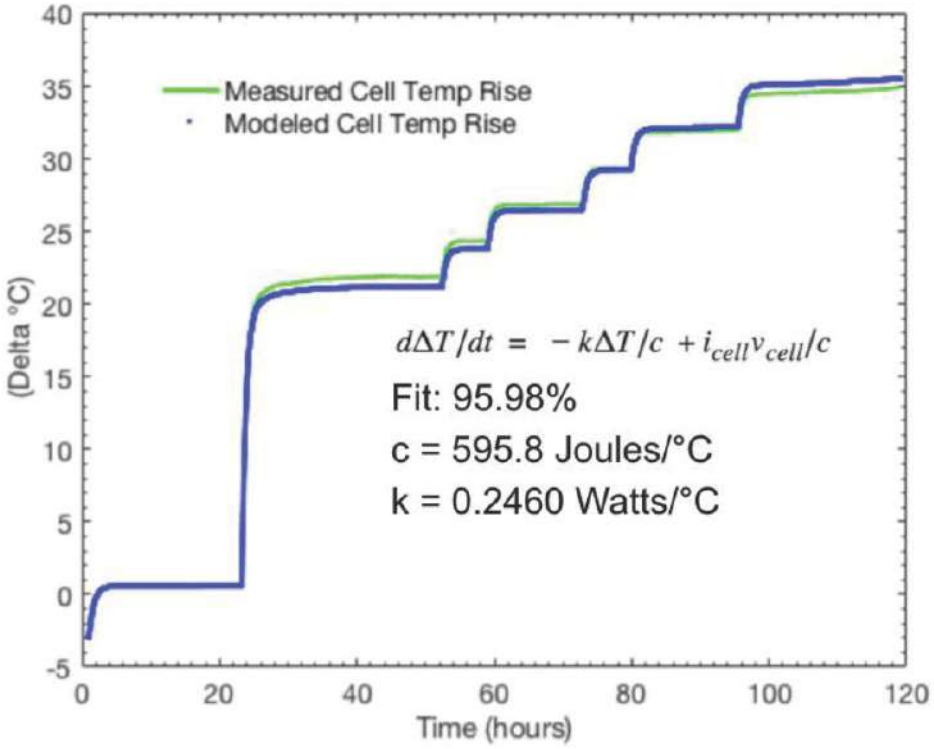

Figure 19. Measured and modeled cell temperature difference time series using linear calibration.

affect the cell temperature. This is the assumption adopted in the calibration used by Letts. This assumption entails a minor modification to the first model, namely,

$$\mathrm{d}\Delta T/\mathrm{d}t = -k\Delta T/c + i_{\mathrm{cell}}(v_{\mathrm{cell}} - v_0)/c,$$

where $v_0 = 1.53$ V is the thermoneutral voltage for D_2O. Figure 20 shows the measured and modeled cell temperature difference time series. As before, the model was fit using the Matlab System Identification Toolbox's grey box model routine greyest.

We see that this model does not fit the data as well as the simpler model; the fit using the model that assumes that recombiner heat escapes through the top of the cell has a normalized root mean square error of >7%, which is over 3% worse than the simple model.

S4.3 Radiation fit to calibration data

One feature common to both of the linear models is that temperature rise is overestimated at high input power. This suggests that heat is leaving the calorimeter via a superlinear process. Given that the calorimeter is constructed from a transparent glass beaker it is a natural choice to add radiative heat transfer to the model to test the hypothesis that radiation is responsible for a portion of the heat exiting the calorimeter. Next we considered the possibility that the

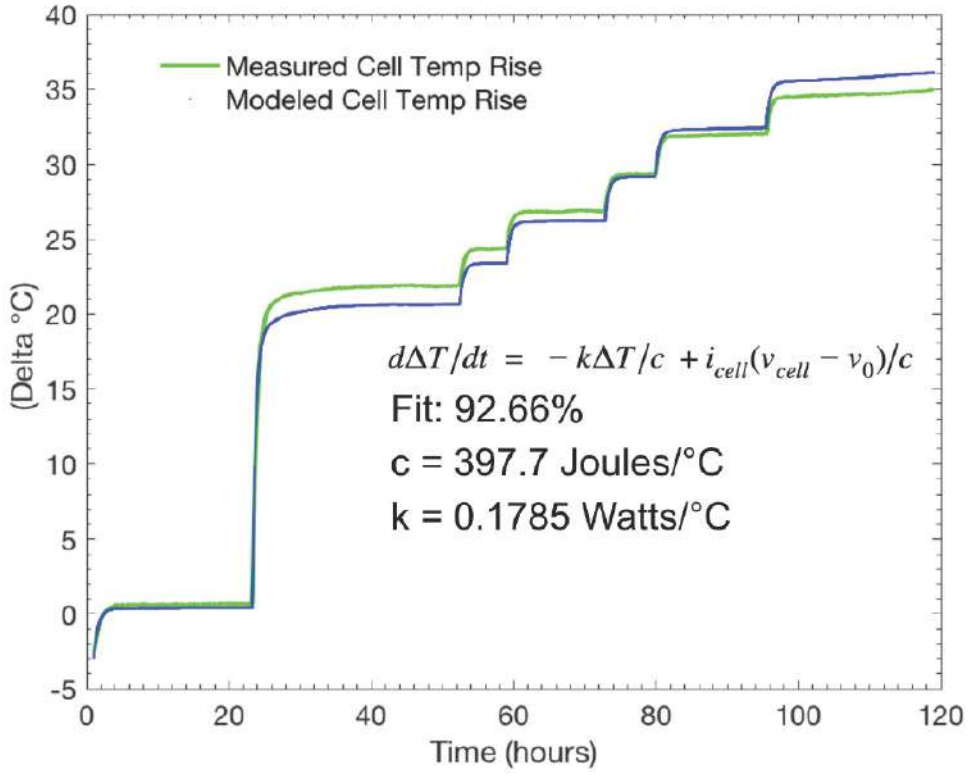

Figure 20. Measured and modeled cell temperature difference time series using linear calibration with subtracted electrolysis power.

calorimeter dynamics are governed by the equation

$$\mathrm{d}\Delta T/\mathrm{d}t = -k_{\mathrm{conc}}\Delta T/c - k_{\mathrm{rad}}(T^4_{\mathrm{cell}} - T^4_{\mathrm{surroundings}}) + i_{\mathrm{cell}}v_{\mathrm{cell}}/c.$$

Note that the terms T_{cell} and $T_{\mathrm{surroundings}}$ are in Kelvin. A more convenient way to write this expression for parameter fitting is

$$\mathrm{d}\Delta T/\mathrm{d}t = -k_{\mathrm{conc}}\Delta T/c\text{-}k_{\mathrm{rad}}[(\Delta T + T_{\mathrm{surroundings}})^4 - T^4_{\mathrm{surroundings}}] + i_{\mathrm{cell}}v_{\mathrm{cell}}/c,$$

because this form expresses the system as a differential equation with a single state (ΔT) with two inputs ($i_{\mathrm{cell}}v_{\mathrm{cell}}$ and $T_{\mathrm{surroundings}}$) and three parameters ($c$, k_{con} and k_{rad}).

Figure 21 shows the measured and modeled ΔT using the nonlinear model. The fitting was done using the Matlab function nlgreyest.

The normalized root mean square error metric for this model is 0.67% which compares favorably to both of the linear models. The table below summarizes the results of the three models used on the DLER10 calibration dataset.

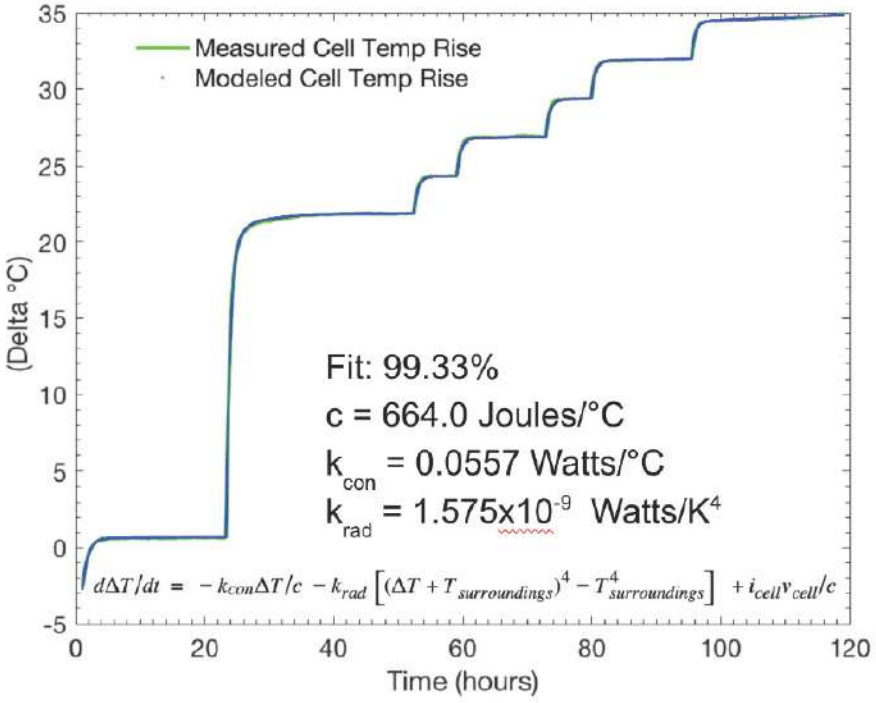

Figure 21. Measured and modeled cell temperature difference time series using the nonlinear model with thermal radiation correction.

Model	Input power (W)	Fit (%)	c (J/°C)	$k_{\rm con}$ (W/°C)	$k_{\rm rad}$(W/K^4)
Linear	$i_{\rm cell}(v_{\rm cell} - v_0)$	92.66	397.7	0.1785	–
Linear	$i_{\rm cell}v_{\rm cell}$	95.98	595.8	0.2460	–
Non-linear	$i_{\rm cell}v_{\rm cell}$	99.33	664.0	0.0557	1.575×10^{-9}

S4.4 Summary of model fitting

By comparing the two linear fits, we see that not only is the assumption that electrolysis energy escapes without detection not well supported; but, that in addition the assumption may underestimate the heat capacity and thermal conductance.

By comparing the $k_{\rm con}$ term of the linear and non-linear models with $i_{\rm cell}v_{\rm cell}$ input power we see an indication that a significant portion of the power leaving the calorimeter does so by radiation.

We chose the DLER10 dataset to illustrate comparative calorimeter models because this dataset was uncharacteristically free of thermometry artifacts, at least for Cell Temperature Sensor 1. One consequence of non-physical thermometry artifacts is that nonlinear parameter estimation methods fail to converge rapidly on a global optimum. For this reason, the calibration model used throughout this report is the linear model with $i_{\rm cell}v_{\rm cell}$ input power.

Acknowledgement

We would like to thank Dennis Letts for his contribution of time and materiel. We are grateful for his assistance. In addition, we would like to thank Coolescence LLC for the contribution of Pd material to test in this experimental campaign.

References

[1] M. Fleischmann, S. Pons and M. Hawkins, Electrochemically induced nuclear fusion of deuterium, *J. Electroanal. Chem.* **201**(1989) 301. Errata, **263** (1990) 187.
[2] M. Fleischmann, S. Pons, M.W. Anderson, L.J. Li and M. Hawkins, Calorimetry of the palladium—deuterium–heavy water system, *J. Electroanal. Chem.* **287** (1990) 293.
[3] S.E. Jones, E.P. Palmer, J.B. Czirr, D.L. Decker, G.L. Jensen, J.M. Thorne, S.F. Taylor and J. Rafelski, Observation of cold nuclear fusion in condensed matter, *Nature* **338** (1989) 737.
[4] M.C.H. McKubre, S. Crouch-Baker, F.L. Tanzella, S.I. Smedley, M. Williams, S. Wing, M. Maly-Schreiber, R.C. Rocha-Fiho, P.C. Searson, J.G. Pronko and D.A. Kohler., Development of advanced concepts for nuclear processes in deuterated metals, TR-104195 Electric Power Research Institute: Palo Alto, 1994.
[5] M.H. Miles, R.A. Hollins, B.F. Bush, J.J. Lagowsi and R.E. Miles, Correlation of excess power and helium production during D_2O and H_2O electrolysis using palladium cathodes, *J. Electroanal. Chem.* **346** (1993) 99.
[6] E. Castagna, M. Sansovini, S. Lecci, A. Rufoloni, F. Sarto, V. Violante, D.L. Knies, K.S. Grabowski, G.K. Hubler, M. McKubre and F. Tanzella, Metallurgical characterization of Pd electrodes employed in calorimetric experiments under electrochemical deuterium loading, In *Proc 14th Int Conf on Condensed Matter Nuclear Science*, Washington, DC, August 10-15, 2008.
[7] P.L. Hagelstein, D. Letts and D. Cravens, Terahertz difference frequency response of PdD in two-laser experiments, *J. Condensed Matter Nucl. Sci.* **3** (2010) 59–76.
[8] D Letts, Highly reproducible LENR experiments using dual laser stimulation, *Current Science* **108** (2015) 559–561 and Supplementary Information.
[9] D.J. Nagel, Scientific and commercial overview of ICCF-19, *Infinite Energy*, July/August 2015.
[10] P.L. Hagelstein, Current status of the theory and modelling effort based on fractionation, presented at *ICCF-19*, Padua, Italy, April 13–17, 2015.
[11] D. Letts, personal communication, 2015.
[12] D. Letts and D. Cravens, Cathode fabrication methods to reproduce the Letts–Cravens effect, presented at *5th Asti Workshop on Anomalies in Hydrogen/Deuterium loaded Metals*, Asti, Italy, March 19–21 2004.
[13] http://www.ni.com/pdf/manuals/371304g.pdf
[14] ibid P.L. Hagelstein, D. Letts and D. Cravens, Terahertz difference frequency response of PdD in two-laser experiments, *J. Condensed Matter Nucl. Sci.* **3** (2010) 59–76.
[15] An example linear fit to steady state data is included in the Supplemental Information.
[16] P.L. Hagelstein and D.G. Letts, Analysis of some experimental data from the two-laser experiment, *J. Condensed Matter Nucl. Sci.* **3** (2010) 77–92.
[17] P.L. Hagelstein and D. Letts, *JCMNS* 2010, Appendix A.2.1.
[18] M.C.H. McKubre, personal communication.